Vol. 38 (2007) ACTA PHYSICA POLONICA B No 7

BEARING STANDARD MODEL BENCHMARKS TO THE LHC*

J.W. Huston

Department of Physics and Astronomy, Michigan State University
East Lansing, MI 48824, USA

(Received May 25, 2007)

I discuss the importance of understanding Standard Model predictions and results at the LHC during the early running.

PACS numbers: 12.38.–t,12.38.Qk

1. Introduction

The first run of the LHC in 2008 at a center-of-mass energy of 14 TeV will open up an unexplored kinematic regime in which there are great possibilities and expectations for new physics. However, this will also be a period in which both the detectors and the Standard Model physics at the LHC may be poorly understood and in which it may be easy to mistake Standard Model results for new physics. Or even worse, a mis-understanding of Standard Model physics may result in new physics effects being overlooked. Thus, it will be important in the early running of the LHC to establish Standard Model Benchmarks that will serve as a framework in which to search for Beyond the Standard Model effects.

The expectations for LHC physics can be sorted into three categories [1]:

- known-knowns
- known-unknowns
- unknown-unknowns

In the category of known-knowns, I would list the great understanding of the Standard Model that we have gained from our experiences at the Tevatron, HERA and LEP, and (most) of the resultant extrapolations to the LHC. However, the LHC is exploring a new kinematic regime and there

* Presented at the Cracow Epiphany Conference on Precision Physics and Monte Carlos for LHC, Cracow, Poland, 4–6 January 2007.

are some extrapolations for which we are unsure and which must be designated as known-unknowns. And, of course, the items that fall into the third category are currently unknown, hence the name.

Due to the limitations of length, I will concentrate on only a few of the known-knowns and known-unknowns and direct the interested reader to a longer discussion in a recent review article [2].

The most directly relevant experience for the LHC comes from another hadron–hadron collider, the Tevatron. This experience is very useful, but hard interactions at the LHC are not necessarily just "re-scaled" scatterings at the Tevatron. There are small momentum fractions (x) in many key searches leading to:

- a dominance of gluon and sea-quark scattering
- a large phase space for gluon emission and thus for production of extra jets
- in general, intensive QCD backgrounds compared to HERA and the Tevatron.

In addition, many of the scales relating to interesting processes are large compared to the W mass; thus, electroweak corrections can become important even for nominally QCD processes.

2. Parton distribution functions

2.1. Introduction

The calculation of cross sections at the LHC relies upon a knowledge of the distribution of the momentum fraction x of the partons (quarks and gluons) in a proton in the relevant kinematic range. These parton distribution functions (pdfs) cannot be calculated perturbatively but rather are determined by global fits to data from deep inelastic scattering (DIS), Drell–Yan (DY), and jet production at current energy ranges. Two major groups, CTEQ [3] and MRST [4], provide semi-regular updates to the parton distributions when new data and/or theoretical developments become available. In addition, there are also pdfs available from Alekhin [5] and from the two HERA experiments [6–9]. The newest pdfs, in most cases, provide the most accurate description of the world's data, and should be utilized in preference to older pdf sets.

2.2. Pdf uncertainties

In addition to having the best estimates for the values of the pdfs in a given kinematic range, it is also important to understand the allowed range of variation of the pdfs, *i.e.* their uncertainties. There has been a great deal of recent activity on the subject of pdf uncertainties. Two techniques in particular, the Lagrange Multiplier and Hessian techniques, have been used by CTEQ and MRST to estimate pdf uncertainties [10–12]. The Lagrange Multiplier technique is useful for probing the pdf uncertainty of a given process, such as the W cross section, while the Hessian technique provides a more general framework for estimating the pdf uncertainty for any cross section. In addition, the Hessian technique results in tools more accessible to the general user.

In the Hessian method a large matrix (20×20 for CTEQ, 15×15 for MRST), with dimension equal to the number of free parameters in the fit, has to be diagonalized. The result is 20 (15) orthonormal eigenvector directions for CTEQ (MRST) which provide the basis for the determination of the pdf error for any cross section. This process is shown schematically in Fig. 1.

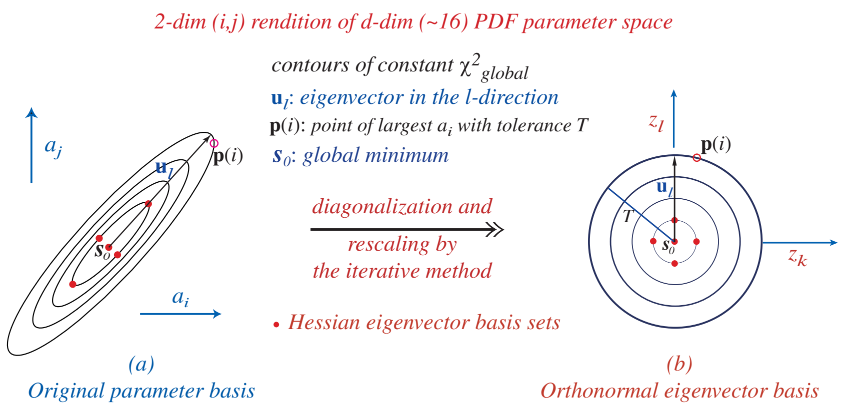

Fig. 1. A schematic representation of the transformation from the pdf parameter basis to the orthonormal eigenvector basis.

The eigenvectors are now admixtures of the 20 pdf parameters left free in the global fit. There is a broad range for the eigenvalues, over a factor of one million. The eigenvalues are distributed roughly linearly as $\log \varepsilon_i$, where ε_i is the eigenvalue for the i-th direction. The larger eigenvalues correspond to directions which are well-determined; for example, eigenvectors 1 and 2 are sensitive primarily to the valence quark distributions at moderate x, a region where they are well-constrained. The theoretical uncertainty on the determination of the W mass at both the Tevatron and the LHC depends primarily on these 2 eigenvector directions, as W production at the Tevatron proceeds primarily through collisions of valence quarks. The most significant eigenvector directions for determination of the W mass at the LHC correspond to larger eigenvector numbers, which are primarily determined by sea quark distributions. In most cases, the eigenvector cannot be directly tied to the behaviour of a particular pdf in a specific kinematic region. Consider a variable X; its value using the central pdf for an error set (say CTEQ6.1M) is given by X_0. X_i^+ is the value of that variable using the pdf corresponding to the "+" direction for eigenvector i and X_i^- the value for the variable using the pdf corresponding to the "−" direction. In order to calculate the pdf error for an observable, a *Master Equation* should be used:

$$\begin{aligned} \Delta X^+_{\max} &= \sqrt{\sum_{i=1}^{N}[\max(X_i^+ - X_0, X_i^- - X_0, 0)]^2} \\ \Delta X^-_{\max} &= \sqrt{\sum_{i=1}^{N}[\max(X_0 - X_i^+, X_0 - X_i^-, 0)]^2}\,. \end{aligned} \tag{2.1}$$

ΔX^+ adds in quadrature the pdf error contributions that lead to an increase in the observable X and ΔX^- the pdf error contributions that lead to a decrease. The addition in quadrature is justified by the eigenvectors forming an orthonormal basis. The sum is over all N eigenvector directions, or 20 in the case of CTEQ6.1. Ordinarily, $X_i^+ - X_0$ will be positive and $X_i^- - X_0$ will be negative, and thus it is trivial as to which term is to be included in each quadratic sum. For the higher number eigenvectors, however, the "+" and "−" contributions may be in the same direction. In this case, only the most positive term will be included in the calculation of ΔX^+ and the most negative in the calculation of ΔX^-. Thus, there may be less than N terms for either the "+" or "−" directions. Either X_0 and $X_i^\pm$ can be calculated separately in a matrix element/Monte Carlo program (requiring the program to be run $2N+1$ times) or X_0 can be calculated with the program and at the same time the ratio of the pdf luminosities (the product of the two pdfs at the x values used in the generation of the event) for eigenvector i ($\pm$) to that of the central fit can be calculated and stored. This results in an effective sample with $2N+1$ weights, but identical kinematics, requiring a substantially reduced amount of time to generate.

It is important to note that the pdf uncertainties derived from the Lagrange Multiplier and Hessian methods correspond only to uncertainties due to the experimental errors for the data used in the global fitting. Theoretical uncertainties can be of an equal size or even larger [12, 13].

2.3. Parton–parton luminosities

It is useful to define differential parton–parton luminosities. Such luminosities, when multiplied by the dimensionless cross section $\hat{s}\hat{\sigma}$ for a given process, provide a useful estimate of the size of an event cross section at the LHC. Below I define the differential parton–parton luminosity $dL_{ij}/d\hat{s}\,dy$

and its integral $dL_{ij}/d\hat{s}$:

$$\frac{dL_{ij}}{d\hat{s}\,dy} = \frac{1}{s}\,\frac{1}{1+\delta_{ij}}\,[f_i(x_1,\mu)f_j(x_2,\mu) + (1 \leftrightarrow 2)]\,. \tag{2.2}$$

The prefactor with the Kronecker delta avoids double-counting in case the partons are identical. The generic parton-model formula

$$\sigma = \sum_{i,j} \int_0^1 dx_1\, dx_2\, f_i(x_1,\mu)\, f_j(x_2,\mu)\, \hat{\sigma}_{ij} \tag{2.3}$$

can then be written as

$$\sigma = \sum_{i,j} \int \left(\frac{d\hat{s}}{\hat{s}}\, dy\right) \left(\frac{dL_{ij}}{d\hat{s}\,dy}\right) (\hat{s}\,\hat{\sigma}_{ij})\ . \tag{2.4}$$

(Note that this result is easily derived by defining $\tau = x_1 x_2 = \hat{s}/s$ and observing that the Jacobian $\partial(\tau,y)/\partial(x_1,x_2) = 1$.)

Eq. (2.4) can be used to estimate the production rate for a hard scattering process at the LHC as follows. Fig. 2 shows a plot of the luminosity function integrated over rapidity, $dL_{ij}/d\hat{s} = \int (dL_{ij}/d\hat{s}\,dy)\,dy$, at the LHC $\sqrt{s} = 14$ TeV for various parton flavour combinations, calculated using the CTEQ6.1 parton distribution functions [3]. The widths of the curves indicate an estimate for the pdf uncertainties. We assume $\mu = \sqrt{\hat{s}}$ for the scale[1].

One can further specify the parton–parton luminosity for a specific rapidity y and $\hat{s}$, $dL_{ij}/d\hat{s}\,dy$. If one is interested in a specific partonic initial state, then the resulting differential luminosity can be displayed in families of curves as shown in Fig. 3, where the differential parton–parton luminosity at the LHC is shown as a function of the subprocess centre-of-mass energy $\sqrt{\hat{s}}$ at various values of rapidity for the produced system for several different combinations of initial state partons. One can read from the curves the parton–parton luminosity for a specific value of mass fraction and rapidity. (It is also easy to use the Durham pdf plotter to generate the pdf curve for any desired flavour and kinematic configuration[2].)

[1] As expected, the gg luminosity is large at low $\sqrt{\hat{s}}$ but falls rapidly with respect to the other parton luminosities. The gq luminosity is large over the entire kinematic region plotted.

[2] `http://durpdg.dur.ac.uk/hepdata/pdf3.html`

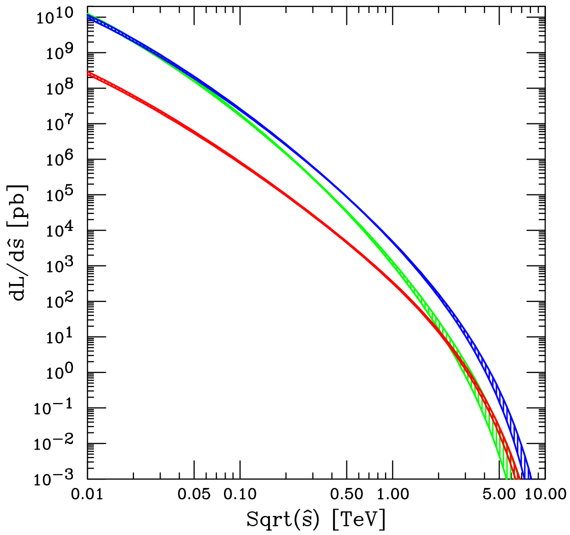

Fig. 2. The parton–parton luminosity $\left[\frac{dL_{ij}}{d\tau}\right]$ in picobarns, integrated over y. Green=gg, Blue=$\sum_i(gq_i + g\bar{q}_i + q_i g + \bar{q}_i g)$, Red=$\sum_i(q_i\bar{q}_i + \bar{q}_i q_i)$, where the sum runs over the five quark flavours d, u, s, c, b. At the highest values of $\sqrt{\hat{s}}$ shown in the figure, the gq luminosity is largest and the $q\overline{q}$ luminosity is smallest.

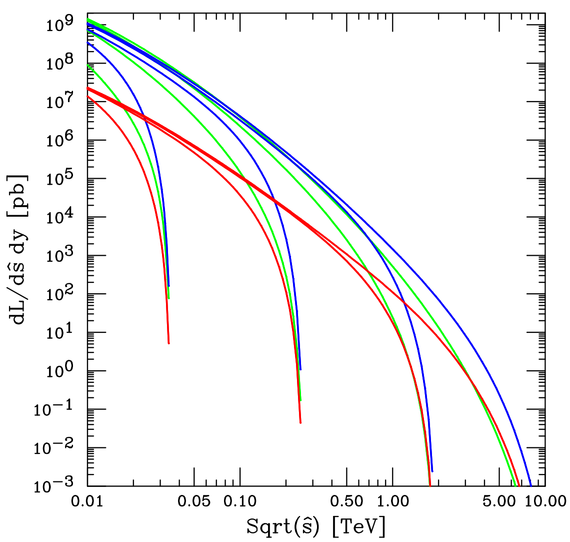

Fig. 3. d(Luminosity)$/dy$ at rapidities (right to left) $y = 0, 2, 4, 6$. Green=gg, Blue=$\sum_i(gq_i + g\bar{q}_i + q_i g + \bar{q}_i g)$, Red=$\sum_i(q_i\bar{q}_i + \bar{q}_i q_i)$, where the sum runs over the five quark flavours d, u, s, c, b. See Ref. [2].

It is also of great interest to understand the uncertainty in the parton–parton luminosity for specific kinematic configurations. Some representative parton–parton luminosity uncertainties, integrated over rapidity, are shown in Figs. 4, 5 and 6. The pdf uncertainties were generated from the CTEQ6.1 Hessian error analysis using the standard $\Delta\chi^2 = 100$ criterion. Except for kinematic regions where one or both partons is a gluon at high x, the pdf uncertainties are of the order of 5–10%. Even tighter constraints will be possible once the LHC Standard Model data is included in the global pdf fits. Again, the uncertainties for individual pdfs can also be calculated online using the Durham pdf plotter.

Often it is not the pdf uncertainty for a cross section that is required, but rather the pdf uncertainty for an acceptance for a given final state. The acceptance for a particular process may depend on the input pdfs due to the rapidity cuts placed on the jets, leptons, photons, *etc.* and the impacts of the varying longitudinal boosts of the final state caused by the different pdf pairs. An approximate "rule-of-thumb" is that the pdf uncertainty for the acceptance is a factor of 5–10 times smaller than the uncertainty for the cross section itself.

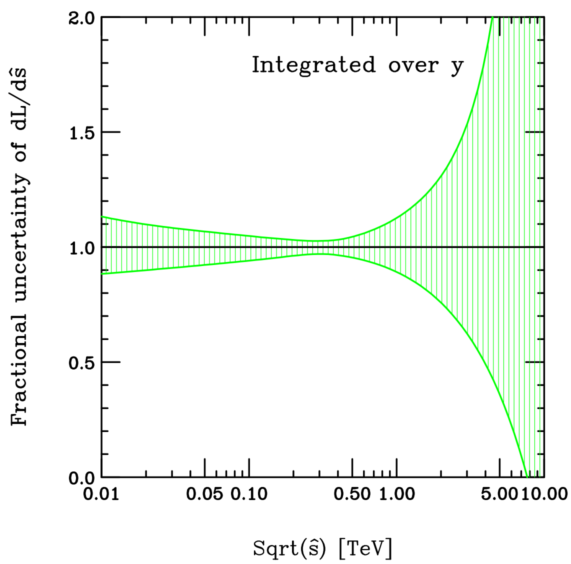

Fig. 4. Fractional uncertainty of the gg luminosity integrated over y.

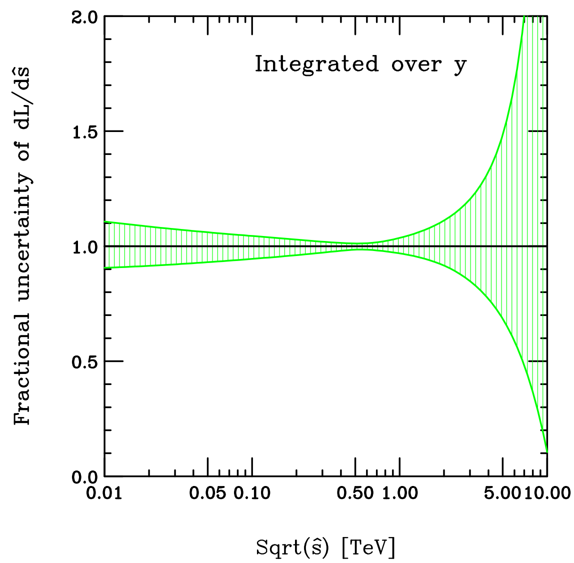

Fig. 5. Fractional uncertainty for the parton–parton luminosity integrated over y for $\sum_i(q_i\bar{q}_i + \bar{q}_i q_i)$, where the sum runs over the five quark flavours d, u, s, c, b.

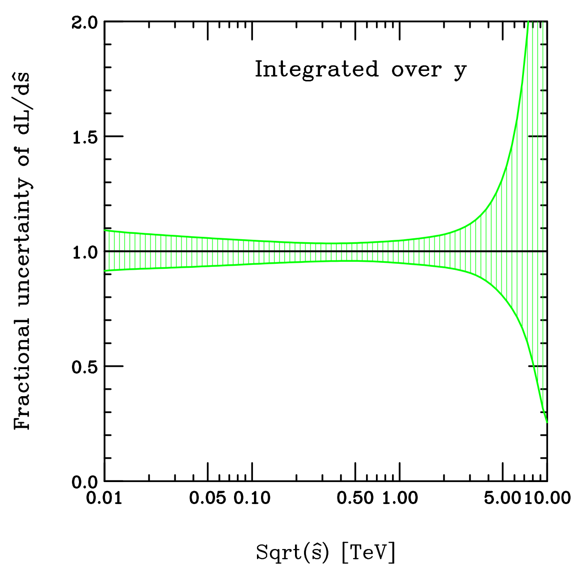

Fig. 6. Fractional uncertainty for the luminosity integrated over y for $\sum_i(q_i\bar{q}_i + \bar{q}_i q_i)$, where the sum runs over the five quark flavours d, u, s, c, b.

2.4. Ratio of LHC and Tevatron luminosities

In Fig. 7, the pdf luminosity curves shown in Fig. 2 are overlaid with equivalent luminosity curves from the Tevatron. In Fig. 8, the ratios of the pdf luminosities at the LHC to those at the Tevatron are plotted. The most dramatic increase in pdf luminosity at the LHC comes from gg initial states, followed by gq initial states and then $q\bar{q}$ initial states. The latter ratio is smallest because of the availability of valence antiquarks at the Tevatron at moderate to large x. As an example, consider chargino pair production with $\sqrt{\hat{s}} = 0.4$ TeV. This process proceeds through $q\bar{q}$ annihilation; thus, there is only a factor of 10 enhancement at the LHC compared to the Tevatron.

Backgrounds to interesting physics at the LHC proceed mostly through gg and gq initial states. Thus, there will be a commensurate increase in the rate for background processes at the LHC.

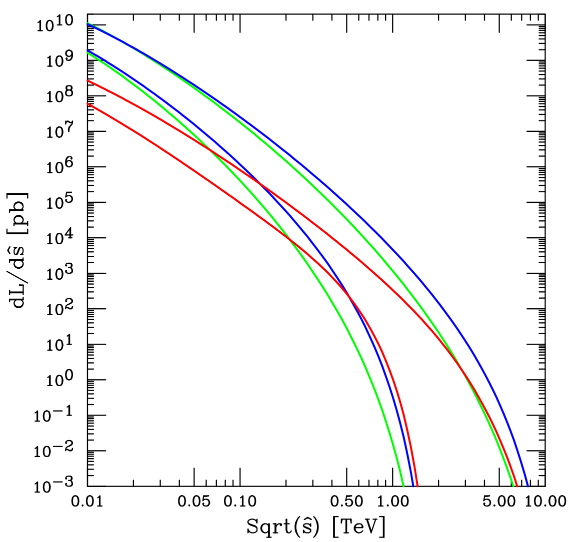

Fig. 7. The parton–parton luminosity $\left[\frac{1}{\hat{s}}\frac{dL_{ij}}{d\tau}\right]$ in pb integrated over y. Green=gg, Blue=$\sum_i(gq_i + g\bar{q}_i + q_i g + \bar{q}_i g)$, Red=$\sum_i(q_i\bar{q}_i + \bar{q}_i q_i)$, where the sum runs over the five quark flavours d, u, s, c, b. The top family of curves are for the LHC and the bottom for the Tevatron. See Ref. [2].

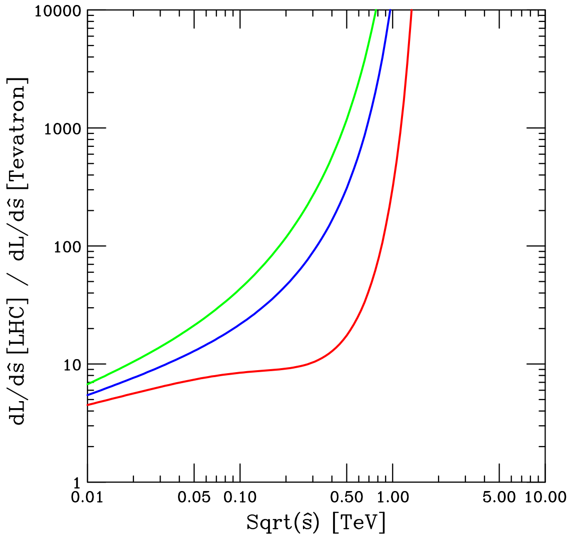

Fig. 8. The ratio of parton–parton luminosity $\left[\frac{1}{\hat{s}}\frac{dL_{ij}}{d\tau}\right]$ in pb integrated over y at the LHC and Tevatron. Green=gg (top), Blue=$\sum_i(gq_i + g\bar{q}_i + q_i g + \bar{q}_i g)$ (middle), Red=$\sum_i(q_i\bar{q}_i + \bar{q}_i q_i)$ (bottom), where the sum runs over the five quark flavours d, u, s, c, b.

3. Next-to-leading order calculations

3.1. Introduction

Although lowest order calculations can in general describe broad features of a particular process and provide the first estimate of its cross section, in many cases this approximation is insufficient. The inherent uncertainty in a lowest order calculation derives from its dependence on the unphysical renormalization and factorization scales, which is often large. In addition, some processes may contain large logarithms that need to be resummed or extra partonic processes may contribute only when going beyond the first approximation. Thus, in order to compare with predictions that have smaller theoretical uncertainties, next-to-leading order calculations are imperative for experimental analyses in Run II of the Tevatron and at the LHC.

3.2. K-factors

The K-factor for a given process is a useful shorthand which encapsulates the strength of the NLO corrections to the lowest order cross section. It is calculated by simply taking the ratio of the NLO to the LO cross section. In principle, the K-factor may be very different for various kinematic regions of the same process. In practice, the K-factor often varies slowly and may be approximated as one number.

However, when referring to a given K-factor one must take care to consider the cross section predictions that entered its calculation. For instance, the ratio can depend quite strongly on the pdfs that were used in both the LO and NLO evaluations. It is by now standard practice to use a NLO pdf (for instance, the CTEQ6M set) in evaluating the NLO cross section and a LO pdf (such as CTEQ6L) in the lowest order calculation. Sometimes this is not the case, instead the same pdf set may be used for both predictions. Of course, if one wants to estimate the NLO effects on a lowest order cross section, one should take care to match the appropriate K-factor.

A further complication is caused by the fact that the K-factor can depend quite strongly on the region of phase space that is being studied. The K-factor which is appropriate for the total cross section of a given process may be quite different from the one when stringent analysis cuts are applied. For processes in which basic cuts must be applied in order to obtain a finite cross section, the K-factor again depends upon the values of those cuts. Lastly, the K-factor depends very strongly upon the renormalization and factorization scales at which it is evaluated. A K-factor can be less than, equal to, or greater than 1, depending on all of the factors described above. Examples are shown in Ref. [2] for a few interesting processes at the Tevatron and the LHC.

3.3. The Les Houches wishlist

A somewhat whimsical experimenter's *wishlist* was first presented at the Run II Monte Carlo workshop at Fermilab in 2001[3]. Since then the list has gathered a great deal of notoriety and has appeared in numerous LHC-related theory talks. It is unlikely that $WWW + b\bar{b} + 3\,$jets will be calculated at NLO soon, no matter the level of physics motivation, but there are a number of high priority calculations, primarily of backgrounds to new physics, that are accessible with the present technology. However, the manpower available before the LHC turns on is limited. Thus, it is necessary to prioritize the calculations, both in terms of the importance of the calculation and the effort expected to bring it to completion.

A prioritized list, determined at the Les Houches 2005 Workshop, is shown in Table I, along with a brief discussion of the physics motivation. Note that the list contains only $2 \to 3$ and $2 \to 4$ processes, as these are feasible to be completed by the turn on of the LHC. First, a few general statements: in general, signatures for new physics will involve high p_{T} leptons and jets (especially b jets) and missing transverse momentum. Thus, backgrounds to new physics will tend to involve (multiple) vector boson production (with jets) and $t\bar{t}$ pair production (with jets). The best manner in

[3] `http://vmsstreamer1.fnal.gov/Lectures/MonteCarlo2001/Index.htm`

which to understand the normalization of a cross section is to measure it; however the rates for some of the complex final states listed here may be limited and (at least in the early days) must be calculated from NLO theory. As discussed at length previously, NLO is the first order at which both the normalization and shape can be calculated with any degree of confidence.

TABLE I

The wishlist of processes for which a NLO calculation is both desired and feasible in the near future.

Process ($V \in \{Z, W, \gamma\}$)	Relevant for
1. $pp \to V\,V+$ jet	$t\bar{t}H$, new physics
2. $pp \to H + 2$ jets	H production by vector boson fusion (VBF)
3. $pp \to t\bar{t}\,b\bar{b}$	$t\bar{t}H$
4. $pp \to t\bar{t} + 2$ jets	$t\bar{t}H$
5. $pp \to V\,V\,b\bar{b}$	VBF$\to H \to VV$, $t\bar{t}H$, new physics
6. $pp \to V\,V + 2$ jets	VBF$\to H \to VV$
7. $pp \to V + 3$ jets	various new physics signatures
8. $pp \to V\,V\,V$	SUSY trilepton searches

Work on most of the processes of Table I are already in progress by several groups, and clearly all of them aim at a setup which allows for a straightforward application to other processes[4].

From an experimentalist's point-of-view, the NLO calculations discussed thus far may be used to understand changes in normalization and/or shape that occur for a given process when going from LO to NLO [18]. Direct comparisons to the data require either a determination of parton-to-hadron corrections for the theory or hadron-to-parton corrections for the data [19]. Furthermore, for multi-parton final states it is also necessary to model the effects of jet algorithms, when two or more partons may be combined into one jet.

4. Sudakov form factors

The Sudakov form factor gives the probability for a parton to evolve from a harder scale to a softer scale without emitting a parton harder than some resolution scale, either in the initial state or in the final state. Sudakov form factors form the basis for both parton showering and resummation. Typically, the details of the form factors are buried inside the interior of such programs. It is useful, however, to generate plots of the initial state Sudakov form factors for the kinematic conditions encountered at both the Tevatron

[4] Processes 2 [16] and 8 [17] have been calculated since the first version of this list was formulated.

and LHC. Such plots indicate the likelihood for the non-radiation of gluons from the initial state partons, and thus conversely for the radiation of at least one such gluon. Thus, they can also serve as a handy reference for the probability of jets from initial state radiation at the LHC. A Sudakov form factor will depend on: (1) the parton type (quark or gluon), (2) the momentum fraction x of the initial state parton, (3) the hard and cutoff scales for the process and (4) the resolution scale for the emission. Several examples are discussed below. These plots were generated with the HERWIG++ parton shower formalism [20, 21].

It is interesting to compare the Sudakov form factors for $t\bar{t}$ production at the Tevatron and LHC. At the Tevatron, $t\bar{t}$ production proceeds primarily (85%) through $q\bar{q}$ with gg being responsible for 15%, with the partons evaluated near an average x value of 0.3. At the LHC, the percentages are roughly reversed (or more precisely 90% for gg) and the scattering takes place at an average x value of a factor of 7 lower (which we approximate here as $x = 0.03$). The relevant Sudakov form factors are shown in Fig. 9, as a function of the minimum transverse momentum of the emitted gluon, at a hard scale of 200 GeV (roughly appropriate for $t\bar{t}$ production).

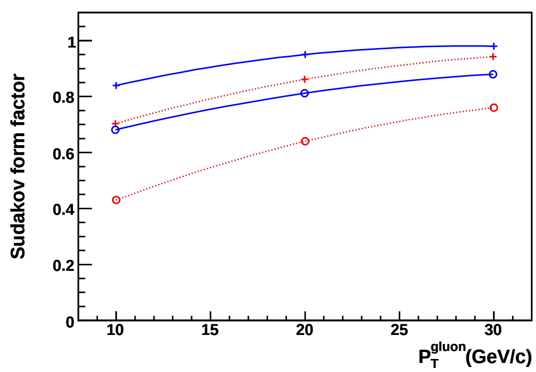

Fig. 9. The Sudakov form factors for initial state quarks and gluons at a hard scale of 200 GeV as a function of the transverse momentum of the emitted gluon. The form factors are for quarks (blue-solid) and gluons (red-dashed) at parton x values of 0.3 (crosses) and 0.03 (open circles).

We can make some rough estimates from these plots. The probability for no gluon of 10 GeV or greater to be radiated from an initial quark leg with $x = 0.3$ is 0.85. The probability for no such gluon to be radiated from either quark leg at the Tevatron is $0.85 \times 0.85 = 0.72$, *i.e.* a 0.28 chance of radiating such a gluon. A similar exercise for two incident gluons of $x = 0.3$ gives a chance of radiating a 10 GeV gluon of 0.51. As the $q\bar{q}$ initial state makes up 85% of the Tevatron cross section, with gg only 15%, the total probability of emitting at least one 10 GeV gluon is 0.3. Using 90% for gg at the LHC and 10% for $q\overline{q}$, gives a 0.8 probability of radiating such a hard gluon.

5. Jets

5.1. Partons and jet algorithms

In the detectors at the LHC, collimated beams of particles are observed. In order to categorize these events, the hadrons are collected into jets using a jet algorithm. To make a comparison with a theoretical calculation of the types we have been discussing, it is necessary to also apply a jet algorithm at the parton level. Ideally, one would like an algorithm which yields similar results at the experimental (hadron) and theoretical (parton) levels. The goal is to characterize the short-distance physics event-by-event, in terms of the jets formed by the algorithm.

There are two essential stages for any jet algorithm. First, the objects belonging to a cluster are identified. Second, the kinematic variables defining the jet are calculated from the objects defining the cluster. The two stages are independent. For the latter stage, using the jet algorithms developed for Run II at the Tevatron, the jet kinematic properties are defined (using a 4-vector recombination scheme) in terms of: $p_{\rm jet}$, $p_{\rm T}^{\rm jet}$, $y^{\rm jet}$ and $\phi^{\rm jet}$.

At the experimental or simulated data level, jet algorithms cluster together objects such as particles or energies measured in calorimeter cells. At the theoretical level, partons are clustered. The goal of a jet algorithm is to produce similar results no matter the level it is applied. For a $2 \rightarrow 2$ LO calculation, a jet consists simply of 1 parton and no jet algorithm is necessary. As more partons are added to a calculation, the complexity of a jet grows and approaches the complexity found either in parton shower Monte Carlos or in data. For all situations in which a jet can consist of more than 1 parton, a completely specified jet algorithm is needed. The clustering algorithms rely on the association of these objects based on transverse momentum (the $k_{\rm T}$ algorithm) or angles (the cone algorithm), relative to a jet axis [22]. For NLO calculations, as for example $W + 2$ jets, a jet can consist of either 1 or 2 partons.

5.2. Jet algorithms and data

For many events, the jet structure is clear and the jets to which the individual towers should be assigned are fairly unambiguous. However, in other events such as Fig. 10, the complexity of the energy depositions means that different algorithms will result in different assignments of towers to the various jets. This is no problem to the extent that a similar complexity can be matched by the theoretical calculation to which it is being compared. This is the case, for example, for events simulated with parton shower Monte Carlos, but, as discussed above current NLO calculations can place at most 2 partons in a jet.

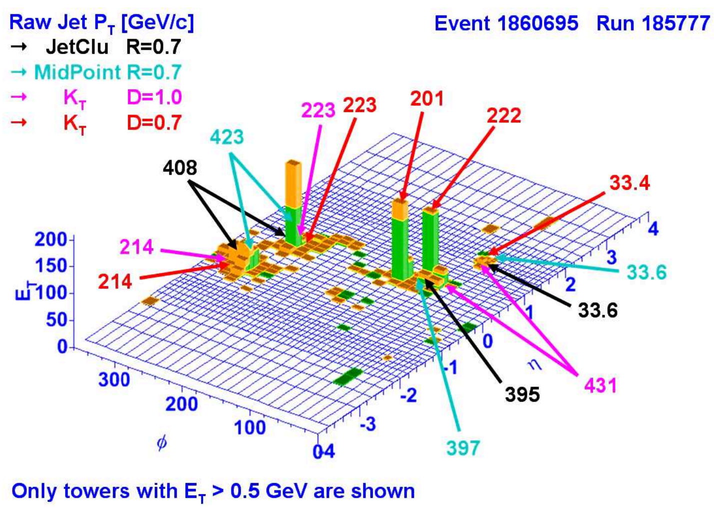

Fig. 10. Impact of different jet clustering algorithms on an interesting event from CDF in Run II.

5.3. *Recent developments*

One of the drawbacks of the k_T algorithm has been its relatively slow speed compared to cone algorithms. The FastkT program has implemented several new methods to greatly decrease the required time and is available in a convenient package [24].

Cone algorithms typically require the use of a seed tower/particle from which to start the jet search, with thresholds on the order of 1 GeV/c. The use of seeds is undesirable from the theoretical point-of-view as they introduce an infra-red sensitivity at higher orders in perturbation theory. The SISCone program has implemented a fast seedless version of the cone algorithm which eliminates this sensitivity [25].

It is often important for experimental (and theoretical) analyses to investigate the choice of jet algorithm and/or parameters on the final physics result. A routine (SpartyJet) has been developed which includes a number of algorithms (including the ones discussed above) and their associated parameters that makes such cross-checks easier. The routine can either be run in stand-alone fashion or incorporated into existing ROOT-based analyses. The routine is available from the website `www.pa.msu.edu/~huston/SpartyJet`.

6. W/Z production

W and Z production have often been suggested as benchmarks for understanding the normalization of other processes at the LHC. Here, I briefly discuss a few aspects of W/Z production at the LHC, with more detailed discussion in Ref. [2].

It is interesting to examine the pdf uncertainties of other processes at the LHC in relation to the pdf uncertainty for W production. The understanding gained may help to reduce the theoretical uncertainties for these processes.

In Fig. 11, we present cross section predictions for Z production at the LHC, calculated using the 41 CTEQ6.1 pdfs. The cross section for Z production at the LHC is highly correlated with the cross section for W production. Both are sensitive to the low x quark pdfs, at a similar x value, which are driven by the gluon distribution at a slightly higher x value.

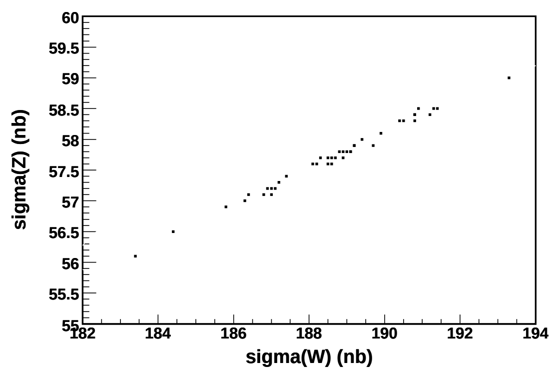

Fig. 11. The cross section predictions for Z production versus the cross section predictions for W production at the LHC plotted using the 41 CTEQ6.1 pdfs.

The rapidity distributions for W^+ and W^- production at LO, NLO and NNLO are shown in Fig. 12, while similar distributions for the Z are shown in Fig. 13. The widths of the curves indicate the scale uncertainty for the cross section predictions. As for the inclusive W and Z cross sections, the scale dependence greatly decreases from LO to NLO to NNLO. There is a sizeable increase in the cross sections from LO to NLO, and a slight decrease (and basically no change in shape) in the cross sections from NLO to NNLO. The change from NLO to NNLO is within the NLO scale uncertainty band.

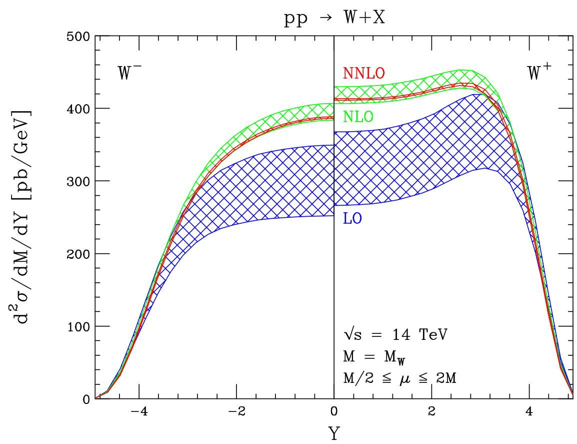

Fig. 12. The rapidity distributions for W^+ and W^- production at the LHC at LO, NLO and NNLO.

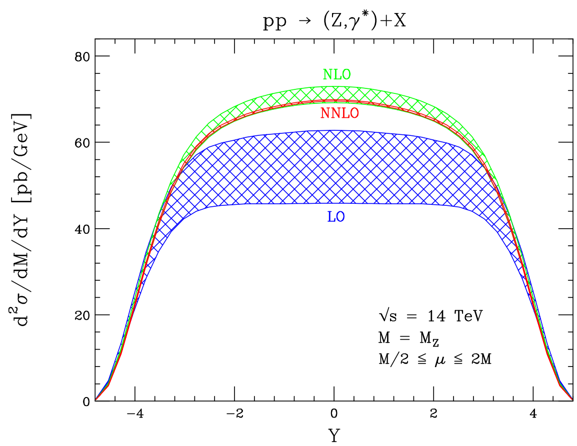

Fig. 13. The rapidity distributions for Z production at the LHC at LO, NLO and NNLO.

The transverse momentum distributions for W and Z production at the LHC are also important to understand. Z production will be one the Standard Model benchmark processes during the early running of the LHC. At low transverse momenta, the distributions are dominated by the effects of multiple soft gluon emission, while at higher p_{T}, hard gluon emission is the major contribution. In Fig. 14, the Z p_{T} distributions at the Tevatron and LHC are shown using predictions from ResBos.

The transverse momentum distribution at the LHC is similar to that at the Tevatron, although somewhat enhanced at moderate transverse momentum values. There is a larger phase space for gluon emission of incident quarks at $x = 0.007$ (Z production at the LHC) than for incident quarks at $x = 0.05$ (Z production at the Tevatron) and the enhancement at moderate transverse momentum is a result of this. There is still substantial influence of the non-perturbative component of the parton transverse momentum near the peak region of the Z transverse momentum distribution [26].

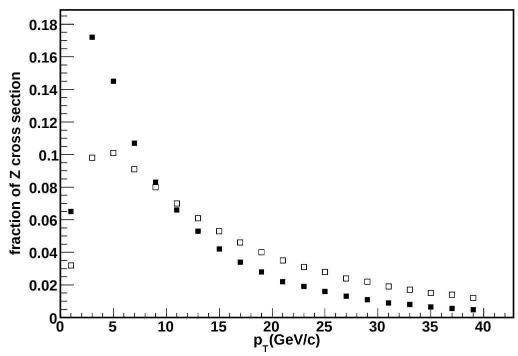

Fig. 14. Predictions for the transverse momentum distributions for Z production at the Tevatron (solid squares) and LHC (open squares).

An analysis of semi-inclusive deep-inelastic scattering hadroproduction suggests a broadening of transverse momentum distributions for x values below 10^{-3} to 10^{-2} [27]. The p_{T} broadening at small x may be due to x-dependent higher order contributions (like BFKL [28–31]) not included in current resummation formalisms. Such contributions are important when $\log Q^2 \ll \log(1/x)$. The BFKL formalism resums terms proportional to $\alpha_s \log(1/x)$, retaining the full Q^2 dependence. The BFKL corrections would have a small impact at the Tevatron (except perhaps for W/Z production in the forward region) but may affect the predictions for $W/Z/$Higgs p_{T} distributions for all rapidity regions at the LHC. The p_{T} broadening can be modeled in the Collins–Soper–Sterman formalism [32] by a modification of the impact parameter-dependent parton densities. The p_{T} shifts for the W and Z transverse momentum distributions at the LHC are shown in Fig. 15 [33]. The observed shifts would have important implications for the measurement of the W boson mass and a measurement of the W/Z p_{T} distributions will be one of the important early benchmarks to be established at the LHC.

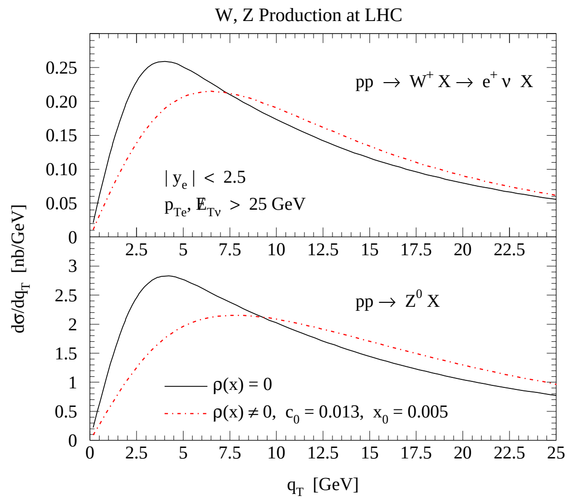

Fig. 15. The predictions for the transverse momentum distributions for W and Z production with and without the p_{T}-broadening effects.

7. Top production

As at the Tevatron, $t\bar{t}$ production at the LHC proceeds through both $q\bar{q}$ and gg initial states. Consider a specific value of $\sqrt{\hat{s}}$ of 0.4 TeV (near $t\bar{t}$ threshold); from Fig. 8, the $q\bar{q}$ annihilation component is only a factor of 10 larger at the LHC than at the Tevatron. The gg component, on the other hand, is over a factor of 500 larger, leading to (1) the large dominance of gg scattering for top pair production at the LHC, in contrast to the situation at the Tevatron and (2) a total $t\bar{t}$ cross section a factor of 100 larger than at the Tevatron. Interestingly, as shown in Fig. 16, the cross section for $t\bar{t}$ production is anti-correlated with the W cross section. An increase in the W cross section is correlated with a decrease in the $t\bar{t}$ cross section and *vice versa*. This is due to the dominance of the gg fusion subprocess for $t\bar{t}$ production, while W production is still predominantly quark–antiquark. An increase in the gluon distribution in the x range relevant for $t\bar{t}$ production leads to a decrease in the quark distributions in the (lower) x range relevant for W production. In fact, the extremes for both cross sections are produced by CTEQ6.1 eigenvector 5 (pdfs 9 and 10) which is most sensitive to the low x behaviour of the gluon distribution.

It is also evident that because of the higher percentage of gg production and the lower average x of the incident partons, the jet multiplicity will be significantly higher for $t\bar{t}$ production at the LHC than at the Tevatron. Consider the production of a pair of top quarks in association with an additional jet at the LHC. Defining the cross section for this process to

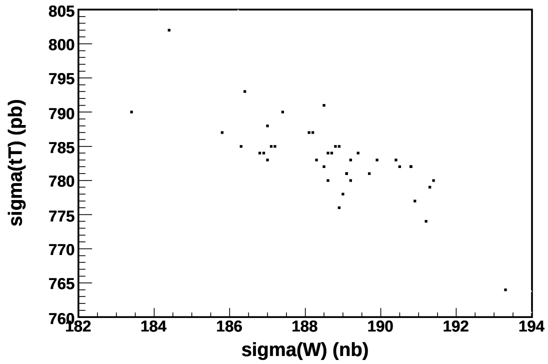

Fig. 16. The cross section predictions for $t\bar{t}$ production *versus* the cross section predictions for W production at the LHC plotted using the 41 CTEQ6.1 pdfs.

only include events with a jet of transverse momentum greater than some minimum value, $p_{\rm T,min}$, yields the dependence on $p_{\rm T,min}$ shown in Fig. 17. Overlaid on this figure is the cross section for top pair production at LO and NLO, which clearly has no dependence on the parameter $p_{\rm T,min}$. As the minimum jet transverse momentum is decreased the cross section for $t\bar{t}$+jet production increases rapidly and in fact saturates the total LO $t\bar{t}$ cross section at around 28 GeV. On the one hand, this appears to be a failing of the leading order predictions. When the $t\bar{t}$ rate is calculated at NLO the cross section increases and the saturation does not occur until around 18 GeV (and presumably higher orders still would relax it further). On the other hand transverse momenta of this size, around 20 GeV, are typical values used to define jets in the LHC experiments. Based on these results, one might certainly expect that jets of these energies might often be found in events containing top quark pairs at the LHC.

The W+jets background to $t\bar{t}$ production proceeds primarily through the gq channel and so receives a factor of 500 enhancement. Thus, the signal to background ratio for $t\bar{t}$ production in a lepton + jets final state is significantly worse at the LHC than at the Tevatron, if the same cuts on the jet transverse momenta as at the Tevatron are used. Thus, the jet cuts applied to $t\bar{t}$ analyses at the LHC need to be set larger than at the Tevatron in order, (1) to reduce the backgrounds from $W + 4$ jet production relative to the lepton + 4 jets final state from $t\bar{t}$ decay, (2) to reduce the number of jets produced by ISR in $t\bar{t}$ events, and (3) to reduce the likelihood of additional jets produced by fluctuations in the underlying event. The signal to background for $t\bar{t}$ is substantially improved at the LHC by increasing the minimum transverse momentum cut for each jet from 15 GeV (Tevatron) to

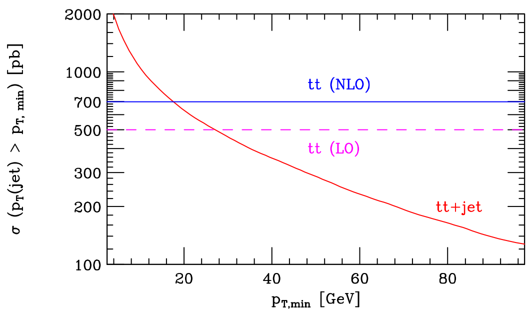

Fig. 17. The dependence of the LO $t\bar{t}$+jet cross section on the jet-defining parameter $p_{\mathrm{T,min}}$, together with the top pair production cross sections at LO and NLO.

30 GeV (CMS) or 40 GeV (ATLAS). The cross section for the production of the lowest p_{T} jet in $W+4$ jet events falls roughly as $1/p_{\mathrm{T}}^{n}$ (where n is in the range 2.5–3) while the distribution for the 4th jet transverse momentum is essentially flat from 15–40 GeV. The background is reduced by a factor of 15 while the signal is reduced by a factor of 5. This reduction in signal is acceptable because of the large $t\bar{t}$ cross section available at the LHC. There are 2.5 million $t\bar{t}$ pairs produced with a lepton + jets final state for a $10\mathrm{fb}^{-1}$ data sample. The requirement for two of the jets to be tagged as b-jets (and the kinematic cuts on the jets (40 GeV) and on the lepton and missing transverse momentum) reduces the event sample to $87,000$, but with a signal to background ratio of 78. A requirement of only one b-tag reduces the signal/background ratio to 28 but with a data sample a factor of 3 larger.

8. Inclusive jet production

The increase of the centre-of-mass energy to 14 TeV at the LHC will result in a dramatically larger accessible kinematic range. Inclusive jet cross sections can be measured out to transverse momentum values of order 4 TeV in the central region and 1.5 TeV in the forward region. The predictions with the CTEQ6.1 central pdfs and the 40 error pdfs are shown in Fig. 18 and 19 for three different rapidity regions [3]. The cross sections were generated with a renormalization and factorization scale equal to $p_{\mathrm{T}}^{\mathrm{jet}}/2$. The cross section predictions have a similar sensitivity to the error pdfs as do the jet cross sections at the Tevatron for similar x_{T} values, and the uncertainties on the predicted cross sections remain up to a factor of 2 at the highest p_{T} values. Measurements of the jet cross section over the full rapidity range at the LHC will serve to further constrain the high x gluon pdf and distinguish between possible new physics and uncertainties in pdfs.

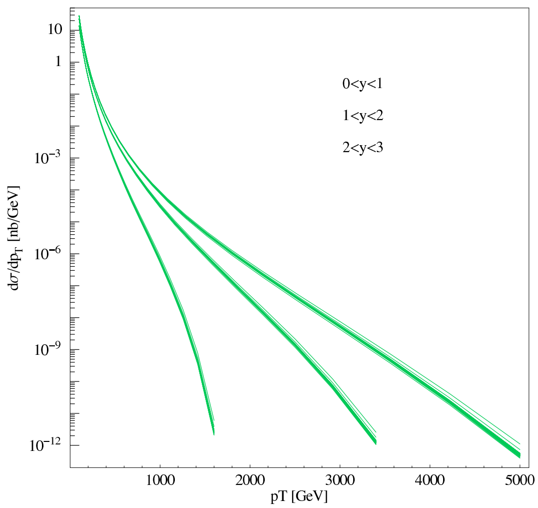

Fig. 18. Inclusive jet cross section predictions for the LHC using the CTEQ6.1 central pdf and the 40 error pdfs.

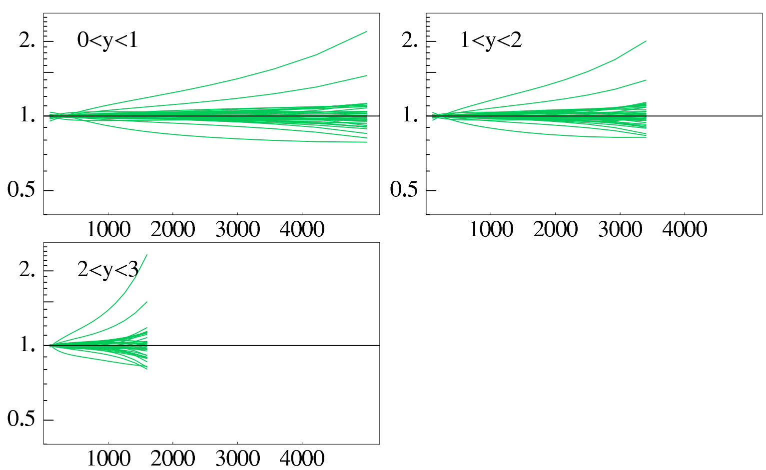

Fig. 19. The ratios of the jet cross section predictions for the LHC using the CTEQ6.1 error pdfs to the prediction using the central pdf. The extremes are produced by eigenvector 15.

It is useful to plot the K-factors (the ratio of the NLO to LO cross sections) for the three different rapidity intervals shown above. As discussed previously, the value of the K-factor is a scale-dependent quantity; the K-factors shown in Fig. 20 are calculated with the nominal scale of $p_T^{\rm jet}/2$. The K-factors have a somewhat complicated shape due to the interplay between the different subprocesses comprising inclusive jet production and the behaviours of the relevant pdfs in the different regions of parton momentum fraction x. In the central region, the K-factor is within 10% of unity for the observable range. There are no new parton–parton subprocesses that contribute at NLO but not at LO. Thus a LO prediction, using the NLO CTEQ6.1 pdfs, will reproduce fairly closely the NLO calculation. For rapidities between 1 and 2, the K-factor is within 20% of unity, dropping below one at higher transverse momentum. For forward rapidities, the K-factor drops almost immediately below one, due to the behaviour of the high-x pdfs that contribute to the cross section in this region. There is nothing wrong with the NLO prediction in this region; its relationship to the LO cross section has just changed due to the kinematics. LO predictions in this region will provide an overestimate of the NLO cross section.

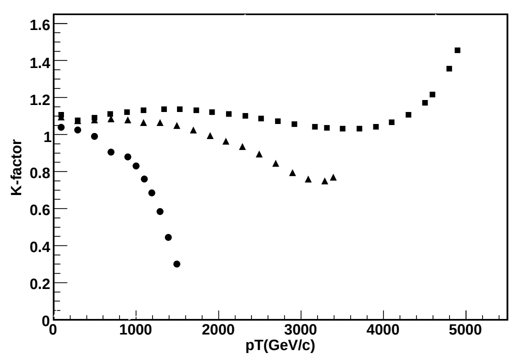

Fig. 20. The ratios of the NLO to LO jet cross section predictions for the LHC using the CTEQ6.1 pdfs for the three different rapidity regions (0–1 (squares), 1–2 (triangles), 2–3 (circles)).

The jets in the upper range of transverse momentum values at the Tevatron are very collimated. This will be even more the case at the LHC, where in the multi-TeV range, a large fraction of the jet's momentum will be contained in a single calorimeter tower. Jet events at the LHC will be much more active than events in a similar p_{T} range at the Tevatron. The majority of the dijet production for the transverse momentum range less than 1 TeV will be with a gg initial state. As discussed previously, the larger colour factor associated with the gluon and the greater phase space available at the LHC for gluon emission will result in an increased production of additional soft jets. In addition, there is an increased probability for the production of "mini-jets" from multiple-parton scattering among the spectator partons. At full design luminosity, on the order of 25 additional minimum bias interactions will be present at each crossing. Such events, either singly or in combination, may create additional jets. As a result, the minimum jet transverse momentum requirement may need to be increased for most analyses; in addition, it may be advantageous to use smaller cone sizes than used for similar analyses at the Tevatron.

9. Conclusions

At turn-on (at 14 TeV), the LHC will access a new energy regime and the possibility of new physics on the first day. For most of the physicists on LHC experiments (and for interested theorists), this will be a once-in-a-lifetime experience. Many of the signals for new physics, such as events with large missing transverse momentum, or a larger than expected event rate with vector bosons, jets etc may also be signs of poorly understood detector systematics and/or Standard Model physics. The rush to find new physics at the LHC should not overshadow first the need to re-discover the Standard Model and to put the resultant cross sections on a firm experimental and theoretical footing; or, in other words, to move as much physics as possible into the known-known category so that true unknown-unknowns can be unveiled.

REFERENCES

[1] D. Rumsfeld, speech at NATO headquarters in Brussels, June 6, 2007.

[2] J.M. Campbell, J.W. Huston, W.J. Stirling, *Rept. Prog. Phys.* **70**, 89 (2007) [hep-ph/0611148].

[3] D. Stump, J. Huston, J. Pumplin, W.K. Tung, H.L.Lai, S. Kuhlmann, J.F. Owens, *J. High Energy Phys.* **0310**, 046 (2003) [hep-ph/0303013].

[4] A.D. Martin, R.G. Roberts, W.J. Stirling, R.S. Thorne, *Phys. Lett.* **B604**, 61 (2004) [hep-ph/0410230].

[5] S. Alekhin, *JETP Lett.* **82**, 628 (2005); *Pisma Zh. Eksp. Teor. Fiz.* **82**, 710 (2005) [hep-ph/0508248].

[6] C. Adloff *et al.* [H1 Collaboration], *Eur. Phys. J.* **C21**, 33 (2001) [hep-ex/0012053].

[7] C. Adloff *et al.* [H1 Collaboration], *Eur. Phys. J.* **C30**, 1 (2003) [hep-ex/0304003].

[8] S. Chekanov *et al.* [ZEUS Collaboration], *Phys. Rev.* **D67**, 012007 (2003) [hep-ex/0208023].

[9] S. Chekanov *et al.* [ZEUS Collaboration], *Eur. Phys. J.* **C42**, 1 (2005) [hep-ph/0503274].

[10] D. Stump *et al.*, *Phys. Rev.* **D65**, 014012 (2002) [hep-ph/0101051].

[11] J. Pumplin *et al.*, *Phys. Rev.* **D65**, 014013 (2002) [hep-ph/0101032].

[12] A.D. Martin, R.G. Roberts, W.J. Stirling, R. S. Thorne, *Eur. Phys. J.* **C28**, 455 (2003) [hep-ph/0211080].

[13] W.K. Tung, H.L. Lai, A. Belyaev, J. Pumplin, D. Stump, C.P. Yuan, *J. High Energy Phys.* **0702**, 053 (2007) [hep-ph/0611254].

[14] A.D. Martin, R.G. Roberts, W.J. Stirling, R.S. Thorne, *Eur. Phys. J.* **C35**, 325 (2004) [hep-ph/0308087].

[15] C. Anastasiou, L.J. Dixon, K. Melnikov, F. Petriello, *Phys. Rev.* **D69**, 094008 (2004) [hep-ph/0312266].

[16] J.M. Campbell, R.K. Ellis, G. Zanderighi, hep-ph/0608194.

[17] A. Lazopoulos, K. Melnikov, F. Petriello, hep-ph/0703273.

[18] J. Campbell, J. Huston, *Phys. Rev.* **D70**, 094021 (2004).

[19] G.U. Flanagan, FERMILAB-THESIS-2005-58.

[20] S. Gieseke *et al.*, hep-ph/0609306.

[21] S. Gieseke, *J. High Energy Phys.* **0501**, 058 (2005) [hep-ph/0412342].

[22] G.C. Blazey *et al.*, hep-ex/0005012.

[23] T.Q.W. Group *et al.*, hep-ph/0610012.

[24] M. Cacciari, G.P. Salam, *Phys. Lett.* **B641**, 57 (2006) [hep-ph/0512210].

[25] G.P. Salam, G. Soyez, hep-ph/0704.0292.

[26] C. Balazs, J. Huston, I. Puljak, *Phys. Rev.* D **63**, 014021 (2001) [hep-ph/0002032].

[27] S. Berge, P. Nadolsky, F. Olness, C.P. Yuan, *Phys. Rev.* **D72**, 033015 (2005) [hep-ph/0410375].

[28] V.S. Fadin, E.A. Kuraev, L.N. Lipatov, *Phys. Lett.* **B60**, 50 (1975).

[29] E.A. Kuraev, L.N. Lipatov, V.S. Fadin, *Sov. Phys. JETP* **44**, 443 (1976); *Zh. Eksp. Teor. Fiz.* **71**, 840 (1976).

[30] E.A. Kuraev, L.N. Lipatov, V.S. Fadin, *Sov. Phys. JETP* **45**, 199 (1977); *Zh. Eksp. Teor. Fiz.* **72**, 377 (1977).

[31] I.I. Balitsky, L.N. Lipatov, *Sov. J. Nucl. Phys.* **28**, 822 (1978); *Yad. Fiz.* **28**, 1597 (1978)].

[32] J.C. Collins, D.E. Soper, G. Sterman, *Nucl. Phys.* **B263**, 37 (1986).

[33] S. Berge, P.M. Nadolsky, F.I. Olness, C.P. Yuan, *AIP Conf. Proc.* **792**, 722 (2005) [hep-ph/0508215].